Available online at www.sciencedirect.com
SCIENCE DIRECT®
Journal of Sound and Vibration 270 (2004) 509–524
JOURNAL OF SOUND AND VIBRATION
www.elsevier.com/locate/jsvi

On the simulation of trailing edge noise with a hybrid LES/APE method

R. Ewert[a,*], W. Schröder[b]

[a] DLR Institute of Aerodynamics and Flow Technology, Technical Acoustics, Lilienthalplatz 7, Braunschweig 38108, Germany
[b] Aerodynamisches Institut, RWTH Aachen, Wüllnerstr. zw. 5 u. 7, Aachen 52062, Germany

Accepted 15 September 2003

Abstract

A hybrid method is applied to predict trailing edge noise based on a large eddy simulation (LES) of the compressible flow problem and acoustic perturbation equations (APE) for the time-dependent simulation of the acoustic field. The acoustic simulation in general considers the mean flow convection and refraction effects such that the computational domain of the flow simulation has to comprise only the significant acoustic source region. Using a modified rescaling method for the prediction of the unsteady turbulent inflow boundary layer, the LES just resolves the flow field in the immediate vicinity of the trailing edge. The linearized APE completely prevent the unbounded growth of hydrodynamic instabilities in critical mean flows.

1. Introduction

Trailing edge noise is simulated using a two-step procedure. In the first step the unsteady compressible flow field in the vicinity of the sharp trailing edge is simulated via a large eddy simulation (LES) [1,2]. In the second step the acoustic field is computed using acoustic perturbation equations (APE) forced by sources determined from the unsteady flow field.

The separation of the analysis of the flow field and the acoustic field offers the possibility to take advantage of the disparity of the turbulent and acoustic length scales at low Mach numbers, where the latter scale with M^{-1} is compared to the former. The mean flow convection and refraction effects are part of the acoustic simulation such that the computational domain for the flow simulation to prescribe the acoustic sources has to comprise only the significant acoustic source region, i.e., it can be kept as small as possible. The integration domain of the acoustic

*Corresponding author. Tel.: +49-531-295-2177; fax: +49-531-295-2320.
E-mail address: roland.ewert@dlr.de (R. Ewert).

0022-460X/$ - see front matter © 2003 Elsevier Ltd. All rights reserved.
doi:10.1016/j.jsv.2003.09.047

computation contains the whole plate. Hence it incorporates diffraction at the leading edge and allows the prediction of directivities.

2. Acoustic perturbation equations

A set of APE has been proposed in Ref. [3] to compute acoustic sound fields with a hybrid method based on a LES of the compressible or the incompressible flow problem. It is shown in Ref. [3] and proved computationally in Ref. [4] that the excitation of instabilities in globally unstable mean flows is prevented due to the properties of the APE system. This important result will be briefly discussed below.

The APE to simulate wave propagation are derived by a flow decomposition into acoustic and non-acoustic quantities, based on a filtering of the non-linear and viscous terms of the Navier–Stokes and continuity equations, respectively, in Fourier/Laplace space [1,3,4]. The APE system for the perturbation variables $(p', \mathbf{u}^a)^{\mathrm{T}}$ gives [3]

$$\frac{\partial p'}{\partial t} + \bar{c}^2 \nabla \cdot \left(\bar{\rho} \mathbf{u}^a + \frac{p'}{\bar{c}^2} \bar{\mathbf{u}} \right) = \bar{c}^2 q_c, \tag{1}$$

$$\frac{\partial \mathbf{u}^a}{\partial t} + \nabla(\bar{\mathbf{u}} \cdot \mathbf{u}^a) + \nabla \left(\frac{p'}{\bar{\rho}} \right) = \mathbf{q}_m \tag{2}$$

with $\bar{c}^2 = \gamma \bar{p}/\bar{\rho}$ the mean flow wave propagation speed. The left-hand side of this system describes wave propagation in a non-uniform mean flow field $\bar{\mathbf{u}}$. Computing the propagation of the acoustic waves, including the convection effects in a time-averaged steady base flow field, allows restriction of the unsteady flow simulation to the immediate vicinity of the source region under consideration, while the mean flow field can be computed using efficient RANS or Euler methods.

Explicit formulations for the source terms q_c and $\mathbf{q}_m$ on the right-hand side of the APE system (1) and (2) are obtained from source filtering [3,5]. As a formal result, it follows that the acoustic velocity perturbations $\mathbf{u}^a$ on the left-hand side of Eqs. (1) and (2) are the irrotational part of the complete perturbation velocities $\mathbf{u}' = \mathbf{u}^a + \mathbf{u}^v$, whereas the sources q_c, $\mathbf{q}_m$ are functions of the solenoidal part $\mathbf{u}^v$. The sources are

$$q_c = -\nabla \bar{\rho} \cdot \mathbf{u}^v - \nabla \cdot [\rho' \mathbf{u}']' + \frac{\bar{\rho}}{c_p} \frac{\bar{D}s'}{Dt}, \tag{3}$$

$$\mathbf{q}_m = -\frac{\partial \mathbf{u}^v}{\partial t} - \nabla(\bar{\mathbf{u}}\mathbf{u}^v) - [\boldsymbol{\omega} \times \mathbf{u}]' - \nabla \frac{(u')^2}{2} + \left[\frac{\nabla \cdot \tau}{\rho} \right]' + T' \nabla \bar{s} - \nabla \bar{T} s' \tag{4}$$

with the substantial derivative $\bar{D}/Dt = \partial/\partial t + \bar{\mathbf{u}} \cdot \nabla$ and $[\cdots]' = [\cdots] - \overline{[\cdots]}$, where the overbar denotes time averaging. Non-linear entropy fluctuations in Eqs. (3) and (4) are not considered. Note that since $\mathbf{u}^a$ on the left-hand side of Eq. (2) is irrotational, i.e., it can be expressed through the gradient of a velocity potential, the curl of the whole left-hand side vanishes and so do all the right-hand side terms, i.e., altogether the terms of Eq. (4) are irrotational. Furthermore, the sources also contain linear terms.

The solenoidal perturbations follow directly from an incompressible flow simulation, which might be sufficient for low Mach number problems to describe the remaining source terms

involving the complete perturbation velocities properly, too. In order to obtain the solenoidal velocity components from the perturbation velocities of a compressible flow simulation, Biot Savart's law has to be used, for instance in 2-D by solving one Poisson equation.

In this work, however, an alternative vortex sound source based on Lamb's vector $\mathbf{L} = \boldsymbol{\omega} \times \mathbf{u}$, which is discussed in the next section, is used. This source vector can be computed easily from a compressible LES simulation and avoids the effort to solve the Poisson equation.

Unlike the filtered source proposed in Ref. [3] the alternative source formulation based on Lamb's vector generates vortical disturbances in the APE system, i.e., $\mathbf{u}^a$ in Eqs. (1) and (2) has to be replaced by $\mathbf{u}'$. Hydrodynamic instabilities are prevented despite using a non-filtered source vector since stability is not obtained by suppressing the excitation of vorticity in the equations through the irrotational source (4), but rather is a property of the governing APE system.

To show this stability property the homogeneous APE system, with dropped sources $q_c, \mathbf{q}_m$, can be recast into an equivalent system, where each equation is related to acoustic and vorticity fluctuations. Entropy fluctuations are *a priori* excluded due to the chosen formulation of Eqs. (1) and (2). The perturbation velocity $\mathbf{u}'$ can be split into an irrotational term plus a remaining part

$$\mathbf{u}' = \boldsymbol{\nabla}\varphi + \mathbf{u}^r. \tag{5}$$

Since it has not demanded $\mathbf{u}^r$ to be solenoidal, the decomposition becomes uniquely defined after imposing the additional condition that the unsteady pressure is expressed only in terms of the unsteady potential φ by

$$p' = -\bar{\rho}\frac{\bar{D}\varphi}{Dt}. \tag{6}$$

Substituting Eqs. (5) and (6) into Eqs. (1) and (2) with $\mathbf{u}^a$ exchanged by $\mathbf{u}'$ and zero q-terms yields

$$L\varphi = \left[\frac{\bar{D}}{Dt}\left(\frac{1}{\bar{c}^2}\frac{\bar{D}}{Dt}\right) - \frac{1}{\bar{\rho}}\boldsymbol{\nabla}\cdot(\bar{\rho}\,\boldsymbol{\nabla})\right]\varphi = \frac{1}{\bar{\rho}}\boldsymbol{\nabla}\cdot(\bar{\rho}\mathbf{u}^r), \tag{7}$$

$$\frac{\partial \mathbf{u}^r}{\partial t} + \boldsymbol{\nabla}(\bar{\mathbf{u}}\cdot\mathbf{u}^r) = 0. \tag{8}$$

The left-hand side of Eq. (7) is a convective term with wave operator L for the acoustic fluctuations expressed through φ. The behavior of the vortical perturbations in the APE system is governed by Eq. (8). Since the APE system is derived to be well suited for the simulation of solely acoustic modes it differs from the linearized Euler equations as it does not possess convection equations for the vortical perturbations.

Hydrodynamic instabilities are excluded if the homogeneous APE system (1), (2) or the equivalent system (7), (8) remain stable.

If the wave operator L, (7), can be proven to be stable, a possible unstable behavior of the operator could only be caused by Eq. (8), due to the growth of vortical perturbations $\mathbf{u}^r$. Now, by taking the curl of Eq. (8) it can be rewritten as

$$\frac{\partial \boldsymbol{\omega}^r}{\partial t} = 0, \tag{9}$$

hence the vorticity remains constant. The wave operator on the left-hand side of Eq. (7) is that of Pierce's approximate wave equation [6], which also was derived by Goldstein in Ref. [7] and recently used in Refs. [8,9]. The wave operator is equivalent to the linearized wave operator of

Möhring's acoustic analogy [10,11], which shows

$$LB = \frac{\bar{D}}{Dt}\left(\frac{1}{\bar{c}^2}\frac{\bar{D}B}{Dt}\right) - \frac{1}{\bar{\rho}}\boldsymbol{\nabla}\cdot(\bar{\rho}\,\boldsymbol{\nabla}B) = -\frac{q_{tot}}{\bar{\rho}}, \tag{10}$$

where B is the total enthalpy and

$$q_{tot} = \frac{\partial}{\partial t}\left(\rho_s\frac{\partial s}{\partial t}\right) + \operatorname{div}\rho_s\mathbf{u}\frac{\partial s}{\partial t} + \operatorname{div}\rho T\boldsymbol{\nabla}s + \operatorname{div}\rho\mathbf{u}\times\boldsymbol{\omega}.$$

As discussed by Howe [12] for homentropic high Reynolds number flows his acoustic analogy [13] agrees with Eq. (10). A great number of various acoustic analogies have been proposed in the past in order to extend Lighthill's acoustic analogy [14] to take into account refraction and convection effects in the wave operator and to identify the real acoustic sources. As discussed by Möhring [10,11] and Bergliaffa et al. [15] the wave operator, L, of Pierce's approximate wave equation and that of Möhring's analogy, respectively, has some unique features. Bergliaffa et al. [15] derived it from an action principle. As outlined by Möhring the wave operator, L, can be shown to be formally self-adjoint. From the self-adjointness, a reciprocity relation for the Green's function associated with L can be derived. Furthermore Möhring [10,11] concludes, from the self-adjointness, the existence of a variational principle such that a conservation law for the acoustic energy can be deduced due to Noether's theorem. From the energy conservation it can be concluded that no instabilities occur by applying the wave operator. This is a remarkable result since it is valid for arbitrary non-uniform mean flows and density gradients. Since the stability of the wave operator L is the necessary condition for the stability of the APE system, the APE system also is stable for arbitrary mean flows, even if non-acoustic perturbations are excited by the source terms.

It may be noted that the linearized Euler equations are not stable for critical mean flows, hence solution of the forced linear equations can diverge as was shown in Ref. [4].

3. Source terms of the APE system

Sources $q_c, \mathbf{q}_m$ of the APE system (1), (2) which can be computed easily from a compressible flow simulation without solving a Poisson equation, are found by rewriting the governing flow equations such that the left-hand side is given by the acoustic perturbation system while the right-hand side is defined by the remaining terms. Although such sources will excite also vorticity disturbances in the APE system, stability is not affected as discussed in the previous section. As shown below the vortex sound source is based on the Lamb vector $\mathbf{L} = \boldsymbol{\omega}\times\mathbf{u}$, i.e., the vorticity-based source term of the acoustic analogies of Powell, Howe and Möhring [10,11,13,16]. The Lamb vector will vanish close to solid boundaries due to the no-slip condition, where the flow simulation generally requires the highest resolution. Hence, the acoustic grid can be coarser than the fluid mechanical grid to properly resolve the acoustic sources. Furthermore, since the APE system does not describe convection of vortical disturbances due to its inherent vorticity equation (9), no CFL restrictions related to non-acoustic modes limit the time step.

In the following the continuity and Navier–Stokes equations in primitive non-linear disturbance formulation are used as governing equations. In order to obtain a system with the

perturbation pressure as an independent variable, the second law of thermodynamics in the first order formulation is used. The non-linear terms containing entropy fluctuations are dropped for convenience. These neglected terms just occur as additional source terms on the right-hand side of the final formulation. The governing equations can be written as

$$\frac{\partial \rho'}{\partial t} + \nabla \cdot (\bar{\rho}\mathbf{u}' + \rho'\bar{\mathbf{u}} + \rho'\mathbf{u}' - \overline{\rho'\mathbf{u}'}) = 0, \tag{11}$$

$$\frac{\partial \mathbf{u}'}{\partial t} + (\bar{\mathbf{u}} \cdot \nabla)\mathbf{u}' + (\mathbf{u}' \cdot \nabla)\bar{\mathbf{u}} + \nabla\left(\frac{p'}{\bar{\rho}}\right) = \mathbf{f} \tag{12}$$

with the momentum source

$$\mathbf{f} = -\left[(\mathbf{u}' \cdot \nabla)\mathbf{u}' - \frac{\nabla \cdot \underline{\tau}}{\rho}\right]' + T'\nabla\bar{s} - s'\nabla\bar{T}, \tag{13}$$

where the perturbation density is connected to the perturbation pressure via

$$p' - \bar{c}^2\rho' = \frac{\gamma\bar{p}}{c_p}s'. \tag{14}$$

In order to derive the particular form of Eq. (12) with the momentum source (13), the enthalpy and entropy gradients using the second law of thermodynamics,

$$\frac{\nabla p}{\rho} = \nabla h - T\nabla s, \tag{15}$$

are substituted for the pressure gradient in the full non-linear momentum equation. Then the equation for the perturbation quantities follow by subtracting the time-averaged momentum equation. Since differentiation and time-averaging can be exchanged, only the gradient of the perturbation enthalpy $\nabla h' = \nabla h - \overline{\nabla h}$ remains in the momentum equation. Furthermore, the terms containing entropy can be rewritten $T\nabla s - \overline{T\nabla s} \approx \bar{T}\nabla s' + T'\nabla\bar{s}$. Finally, the first order formulation of the second law of thermodynamics,

$$h' = \frac{p'}{\bar{\rho}} + \bar{T}s', \tag{16}$$

is substituted for the perturbation enthalpy h'. Now, using the identity

$$(\bar{\mathbf{u}} \cdot \nabla)\mathbf{u}' + (\mathbf{u}' \cdot \nabla)\bar{\mathbf{u}} = \nabla(\bar{\mathbf{u}} \cdot \mathbf{u}') + \boldsymbol{\omega}' \times \bar{\mathbf{u}} + \bar{\boldsymbol{\omega}} \times \mathbf{u}'$$

the left-hand side corresponds to the APE system (1)–(2), with $\mathbf{u}^a$ exchanged by $\mathbf{u}'$, while the right-hand side sources show [3]

$$q_c = -\nabla \cdot [\rho'\mathbf{u}']' + \frac{\bar{\rho}}{c_p}\frac{\bar{D}s'}{Dt}, \tag{17}$$

$$\mathbf{q}_m = -[\boldsymbol{\omega} \times \mathbf{u}]' + T'\nabla\bar{s} - s'\nabla\bar{T} - \nabla\frac{(u')^2}{2} + \left[\frac{\nabla \cdot \underline{\tau}}{\rho}\right]'. \tag{18}$$

In Ref. [17] an acoustic analogy is defined to be "*any noise theory in which the equations of motion for a compressible fluid are rearranged in a way that separates linear propagation effects*". Since the linear APE system plus the above sources follow from the governing flow equations,

where the major linear source terms are expressions in vorticity and entropy in the sense of the above definition, it constitutes an acoustic analogy where one can think of sound being generated by vorticity and entropy inhomogeneities. The source term q_c contains a heat source $\bar{\rho}/c_p\bar{D}s'/Dt$. If only vortex sound is considered, the entropy variations can be dropped. The major vortex source term is the Lamb vector, i.e., $\mathbf{q}_m = -[\mathbf{L}]'$ with $\mathbf{L} = \boldsymbol{\omega} \times \mathbf{u}$. For the computations presented in this paper the non-linear and viscous source terms are not considered.

In order to validate the capability of the proposed source term based on Lamb's vector in conjunction with the APE system to simulate properly acoustic fields the spinning vortex pair is computed. Two-point vortices with circulation Γ and distance $2r_0$ are revolving with relative Mach number $M_r = \Gamma/4\pi r_0 c_\infty$, Fig. 1. The point-like vortices are approximated using a vortex core model based on a Gaussian vorticity distribution with a standard deviation $\sigma \approx r_0$ such that the source becomes

$$\mathbf{q}_m(\mathbf{r}, t) = -\frac{\Gamma^2 \mathbf{e}_r(t)}{8\pi^2\sigma^2 r_0} \sum_{i=1}^{2} (-1)^i \exp\left(-\frac{|\mathbf{r} + (-1)^i \mathbf{r}_0(t)|^2}{2\sigma^2}\right), \quad \sigma \approx r_0$$

with $\mathbf{r} = (x, y)^{\mathrm{T}}$, $\mathbf{r}_0 = r_0\mathbf{e}_r$, and $\mathbf{e}_r = (\cos\theta, \sin\theta)^{\mathrm{T}}$, $\theta = \omega t$. The computational domain has an extension of $-100 \leqslant x/r_0 \leqslant 100$ in the x and y direction. The interior grid consists of 141×141 points with a surrounding sponge layer thickness of 11 points. In order to resolve the vortex source properly the orthogonal grid is clustered close to the origin. The results are compared to a solution based on the matched asymptotic expansion (MAE) given by Müller and Obermeier [18]. Spurious waves can be suppressed effectively by spatially filtering. Fig. 2 shows perfect agreement of the pressure contours of the MAE and the APE solutions for the circulation $\Gamma/(c_\infty r_0) = 1.0$. Fig. 3 shows a comparison of the pressure distribution along the diagonal $x = y$ of the MAE solution with the solutions of the APE system for three different vortex circulations and spinning frequencies, i.e., $\Gamma/(c_\infty r_0) = 0.6, 1.0, 1.6$. The acoustic fields of the APE formulations show very good agreement with the analytical solution for all frequencies.

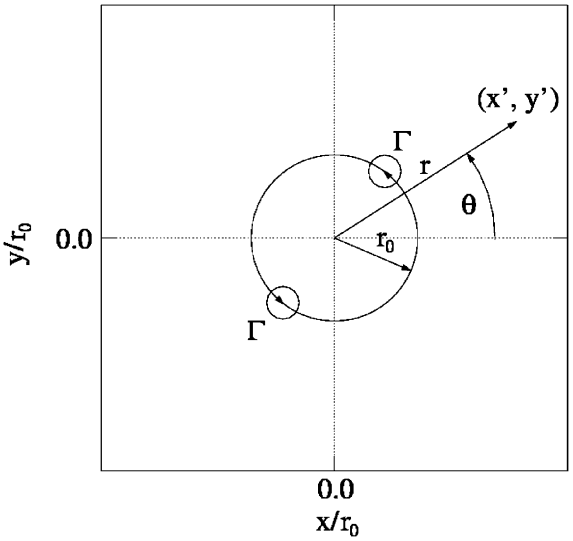

Fig. 1. Sketch of the spinning vortex pair. The distance between both vortices is $2r_0$.

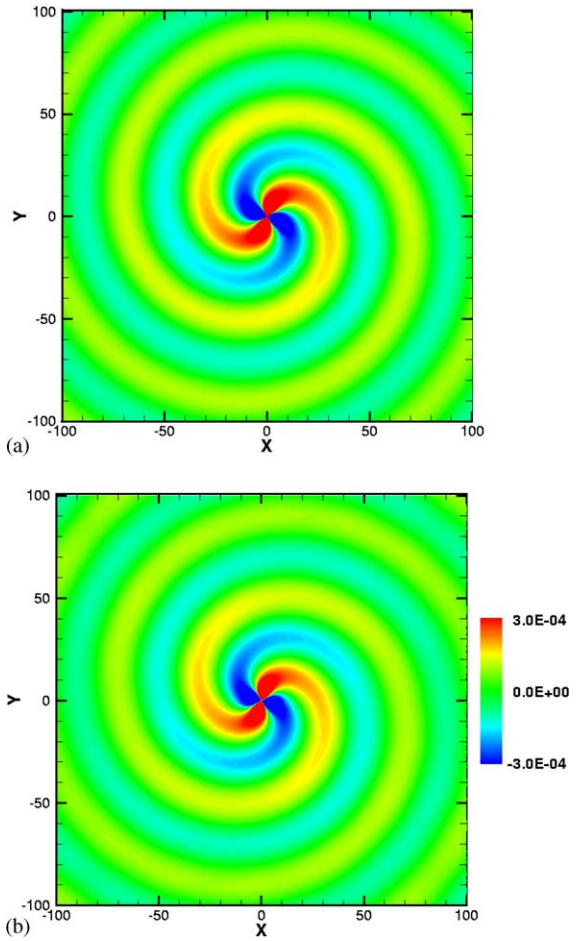

Fig. 2. Comparison of the acoustic pressure contours for a matched asymptotic expansion (MAE) solution (a) and the solution of the APE-4 system with vortex source term (b). $\Gamma/(c_\infty r_0) = 1.0$, $M_r = 0.0796$.

4. Numerical methods

For the spatial discretization of the APE the fourth order dispersion relation preserving (DRP) scheme of Tam and Webb [19] is applied. The DRP scheme is also applied to compute the metric terms of a curvilinear grid such that a consistent discrete system is achieved. The temporal integration is carried out with the fourth order alternating two-step low-dissipation and low-dispersion Runge–Kutta scheme (LDDRK 5-6) proposed by Hu [20].

To suppress spurious high-frequency waves artificial selective damping (ASD) according to Tam and Dong [21] is used. A constant background value of the mesh Reynolds number with a typical value of $1/Re_\Delta = 0.05$ with a slight increase close to boundaries is used. Besides artificial selective damping also explicit commutative filters according to Vasilyev et al. [22] are used. At boundaries one-sided stencils as derived by Vasilyev et al. are imposed. A sponge layer boundary conditions is used at far field boundaries. The formulation of the solid wall boundary conditions is based on the ghost point concept proposed by Tam and Dong [23] in conjunction with body fitted

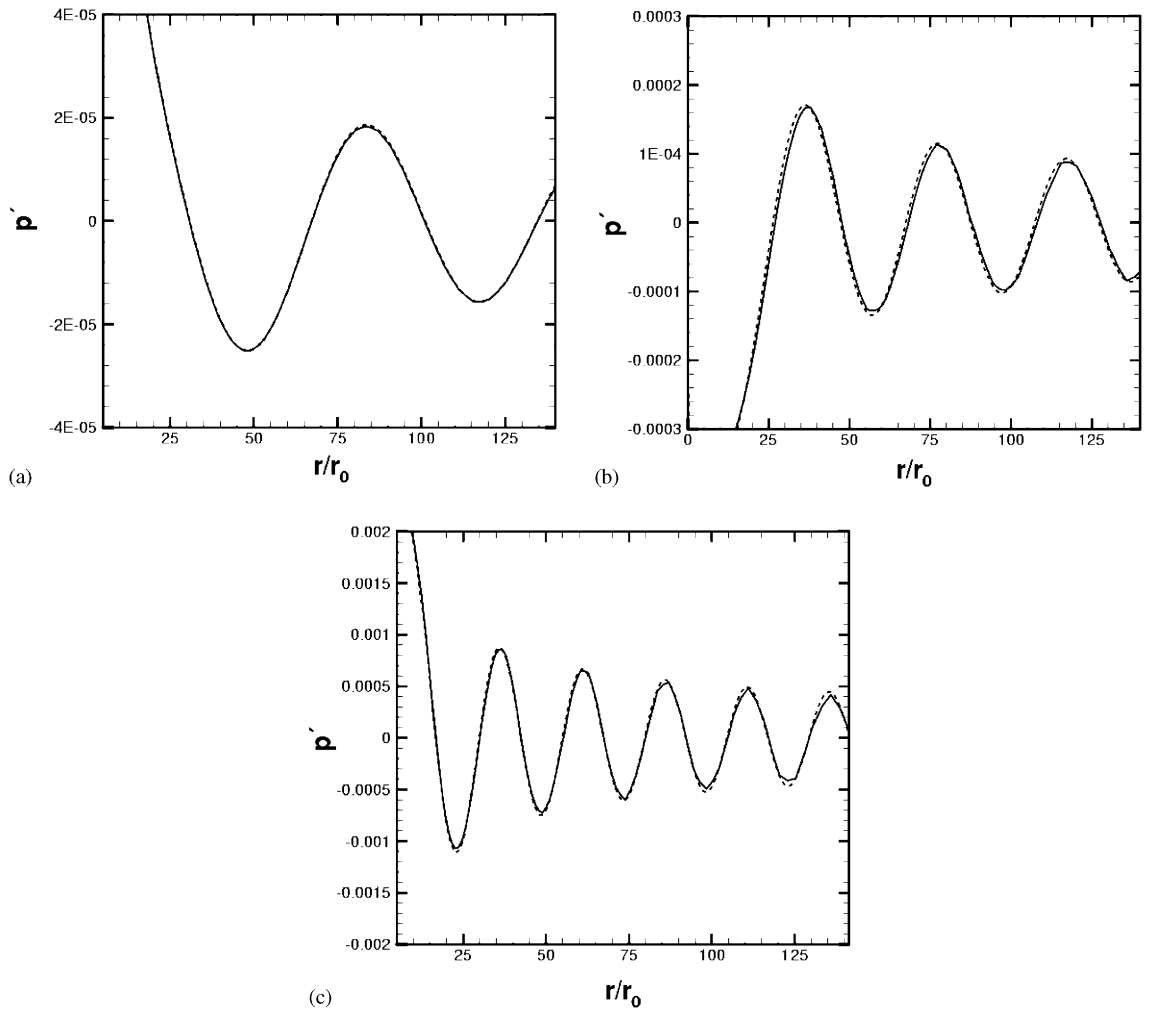

Fig. 3. Pressure distribution p' along $x = y$ for the MAE (– – – –) and APE (——) solution. (a) $\Gamma/(c_\infty r_0) = 0.6$, $M_r = 0.0477$; (b) $\Gamma/(c_\infty r_0) = 1.0$, $M_r = 0.0796$; (c) $\Gamma/(c_\infty r_0) = 1.6$, $M_r = 0.1273$.

grids. The value of the pressure of the ghost point is determined such that the wall normal pressure derivative satisfies the boundary condition, e.g., $\partial p'/\partial n = 0$. It is shown in [23] that the generation of numerical artifacts and high-frequency spurious waves can be reduced significantly using this approach.

5. Simulation of trailing edge noise

5.1. Large-eddy simulation

A large-eddy simulation is performed to simulate the turbulent compressible flow over the trailing edge of a flat plate. The discretization of the convective fluxes of the Navier–Stokes

equations is based on a second order accurate AUSM formulation with a central approximation for the pressure derivative. The viscous stresses are discretized using central differences of second order accuracy. Furthermore, an explicit 5-step Runge–Kutta time stepping scheme of second order accuracy is used for the temporal integration. The coefficients are chosen to maximize the stability of a central scheme. The scheme is described in more detail in Meinke et al. [24]. The flow being simulated corresponds to the experiments conducted by the Universities of Dresden and Stuttgart [25] at a Reynolds number based on the length $l = 0.2$ m of the plate $Re = 4.93 \times 10^5$ and a freestream Mach number $M = 0.15$. The flat plate possesses a thickness $d = 0.35$ mm. To reduce the computational effort while capturing the essential physics, numerical simulations are conducted in a domain that contains only 25% of the total length of the plate. Fig. 4 shows a plane of the LES grid. 17 points in the spanwise direction have been used to yield a grid with 2.22×10^6 points. The spanwise extension is $0.64\delta_0$.

The boundary layer thickness at the inlet is $\delta_0/l = 1/52.228$. The instantaneous inflow data is generated via an auxiliary LES of an adiabatic flat plate boundary layer using a compressible rescaling method. More details of the LES are given in El-Askary et al. [2].

5.2. Sound pressure level (SPL) calculation

Considering a general cylindrical problem, whose 3-D geometry is generated by translation of a 2-D boundary curve in the spanwise direction, i.e., an unswept wing of constant chord length, which is defined by the translation of a 2-D airfoil section, one basic problem arises in any hybrid acoustic method. In the LES the spanwise extension of the computational domain is only in the order of the turbulent length scale and periodic boundary conditions are applied to reduce the computational cost to an acceptable level. Since in low Mach number flows the turbulent length scale is significantly smaller than the acoustical length scale, applying periodic boundary conditions for the compressible problem means to simulate an unphysically correlated acoustic

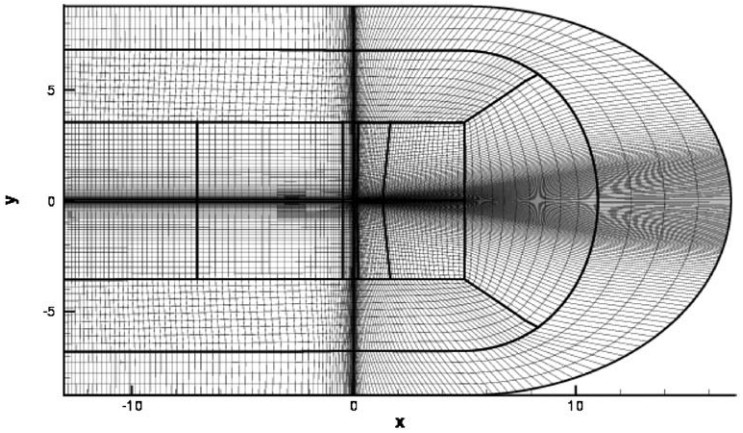

Fig. 4. LES grid, every second grid point is shown. The dimensions are related to the inflow boundary layer δ_0, which scales with $1/52.228$ related to the plate length l.

source in the spanwise direction. This was observed by Manoha et al. [26] by analyzing the acoustic signal contained in the compressible LES of a trailing edge flow. The spanwise unphysically correlated source causes an overprediction of the SPL. Kato et al. [27] state the SPL to be about 14 dB too high. This issue was also discussed by Wang et al. [28]. To avoid such an unphysical correlation it is required to use a spanwise extension in an LES that also resolves the acoustics properly, which is of the order of the acoustic length scale. This means an increase of the grid points of one order of magnitude. However, the flow physics of the hydrodynamic near field is obviously predicted properly via an LES with the usual spanwise extension. Hence, acoustic source terms for a hybrid approach can be predicted properly if the effect of spurious correlation is considered and corrected in the acoustic simulation.

When perturbation equations for the acoustic simulation in 3-D, where the extension in the spanwise z direction equals that of the LES, are applied, in general two types of boundary conditions for the boundaries in the z direction can be used

1. absorbing boundary conditions,
2. periodic boundary conditions.

An acoustic computation with absorbing boundaries in the spanwise direction is equivalent to a 3-D acoustic prediction method, which only considers the sound radiated by the LES domain of length L_S. Hence, SPL corrections have to be applied to take into account a finite span $L \neq L_S$. Furthermore a coherence length L_C that was introduced in Ref. [27] appears as a characteristic length scale of the problem. It is defined by the assumption, that the acoustic field of the source in the spanwise direction is determined by the accumulated signal of slices with width L_C and the source is fully correlated inside each slice but fully uncorrelated outside. For each slice the signal in a receiving point follows by integrating the far field response of all acoustic sources over L_C taking into account phase shifts, while the complete intensity in the receiving point is found by adding up the far field intensities of all slices. If the spanwise length of the cylindrical geometry is small compared to the distance to an observer that is placed in the plane midway between the cylinder ends, where the plane normal is defined by the cylinder axis, the summation of all intensities yields an increase of the intensity in the observer point proportional to the ratio L/L_C compared to one slice of width L_C alone. In general the spanwise extension of the unsteady flow solution L_S has to be chosen such that $L_S \geqslant L_C$ and the SPL corrections follows according to Kato et al. [27]

$$\mathrm{SPL} = \mathrm{SPL}_S + 10\log(L/L_S). \tag{19}$$

However, a computational acoustic domain of small spanwise width yields acoustic waves that leave the domain at very large angles relative to the direction normal to the wall boundary. Most non-reflecting boundary conditions used for computational aeroacoustics will not work properly under these conditions. Therefore, the second case of periodic boundary conditions in the spanwise direction is considered here. Since in low Mach number flows the acoustic length scale is considerably larger than L_S, the source over one slice is compact, hence it can be averaged and smeared over L_S. That is, the 3-D problem with periodic boundary conditions can be described in this compact case by a 2-D acoustic simulation using the 3-D source averaged over L_S. This approach has been applied in this work. The simulated 2-D results have to be corrected to take into account 3-D radiation and a finite span L. According to Oberai et al. [29] for low Mach

number flows the 3-D corrected spectral pressure $\tilde{p}$ follows from the 2-D spectral pressure $\hat{p}$ via

$$\tilde{p}(r,\theta) \approx \hat{p}(r,\theta)\frac{1+\mathrm{i}}{2}\sqrt{\frac{k}{\pi r}}, \tag{20}$$

where k is the wave number, r is the observer distance perpendicular to the cylinder axis, and θ is the polar angle in the 2-D plane. The 2-D problem for $\hat{p}$ is solved using the 3-D acoustic source averaged in the spanwise direction over L_S, hence $\tilde{p}(r,\theta)$ is the sound radiated by one slice of width L_S. Furthermore, for a finite spanwise extension of the cylindrical geometry L the additional correction (19) has to be used where SPL_S denotes the sound pressure levels that follow from $|\tilde{p}|$. Note that all the corrections to the 2-D solution do affect the final spectral SPL distribution, however, have no impact on the θ-dependent directivity.

5.3. Acoustic simulation

The acoustic grid is shown in Fig. 5. The flat plate extends from -1 to 0 and the finite thickness is resolved. The grid is clustered in the wake of the plate to resolve properly the source term. To compute the acoustic source terms in Eq. (18) 503 time levels of the LES have been sampled with a time increment of $\Delta t = 4 \times 10^{-3}$ (reference time $t_{ref} = l/c_\infty$, plate length l). With 20 points per period, this is sufficient to resolve frequencies up to 21 kHz, while the lowest resolution is

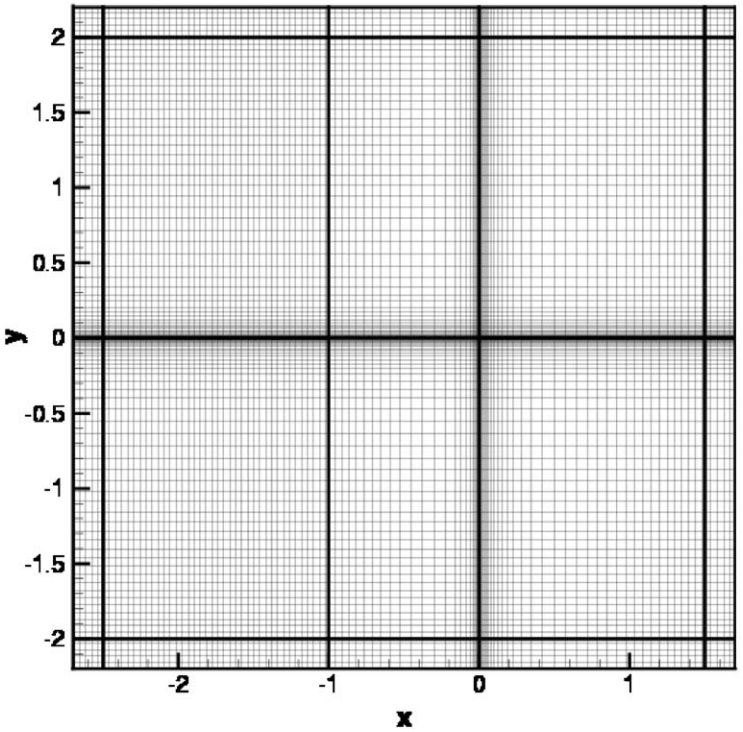

Fig. 5. Acoustic grid scaled with the plate length l, every fourth grid point is shown.

according to the number of time levels in the order of 800 Hz, i.e., the frequency band resolved by the measurements [25] is covered. Due to the fine grid resolution of the LES close to the plate surface, the temporal resolution of the LES is much finer, such that only every 160th time step is used.

Fig. 6 shows snapshots of the source terms in Eq. (18). The quantitative comparison evidences that the main contribution to the source term comes from the y component. The visible vortical structures mainly convect in the downstream direction, where the temporal resolution of the acoustic simulation is sufficient to resolve the source term properly. Note that the source based on Lamb's vector is small close to the wall due to the no-slip boundary condition, where the LES has its finest resolution. The upper half-planes in Fig. 6 show the acoustic grid in the vicinity of the plate. The acoustic grid possesses 2×10^5 points, 17585 of which are located in the LES domain. The source term is computed on the LES grid and then bilinearly interpolated onto the acoustic grid. Entropy fluctuations are neglected in the source computation.

To suppress spurious acoustic signals at in- and outflow boundaries of the LES domain damping zones are used. Since the LES domain is enclosed by a C-shaped sponge layer (Fig. 4) a natural damping zone is obtained at the outflow boundary where the source will decay to zero. At the inflow boundary the computed source is weighted over a width $d = 0.15$.

Figs. 7 and 8 show a snapshot of the pressure field generated at the trailing edge for $T = 3$. Depicted are simulations for the acoustic grid of Fig. 5 and for an acoustic grid with the grid refinement factor of 1.5 for each coordinate direction. Acoustic waves that are generated at the trailing edge are apparent. No spurious sound sources, e.g., from the LES inflow boundary located at $x = -0.25$, are visible. The pressure contours of the coarse and the fine grid simulation evidence a grid-independent solution. Fig. 9(a) shows the directivity $\Phi^{1/2}(\theta, r, kl)$, with Φ being the non-dimensional power spectral density (PSD) of $\overline{p'^2}$, for four different frequencies and a circle centered at the trailing edge with radius $r = 1.5$. The definition of

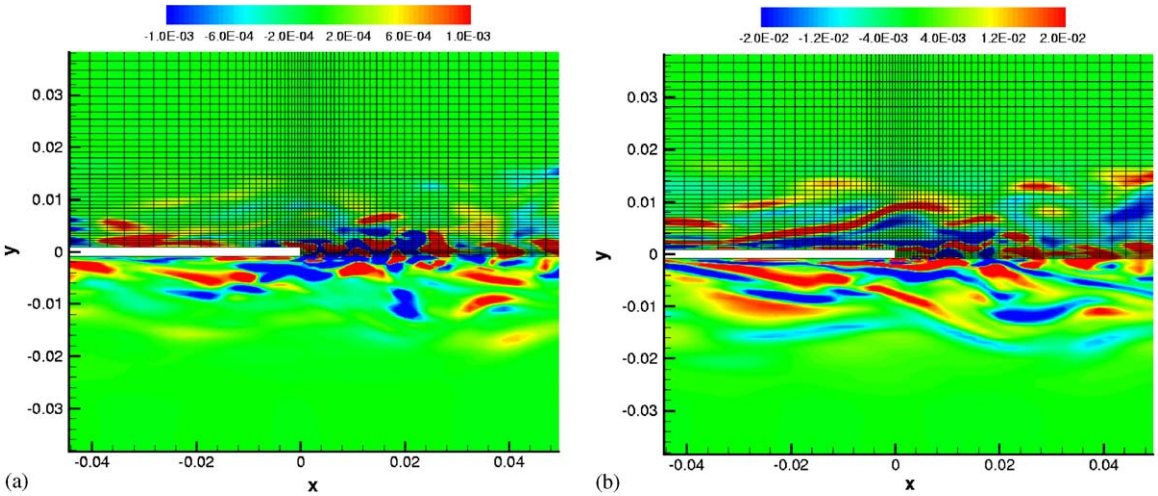

Fig. 6. APE source terms $\mathbf{L}' = [\boldsymbol{\omega} \times \mathbf{u}]' = (L'_x, L'_y)^{\mathrm{T}}$, L'_x (a), L'_y (b), and CAA grid.

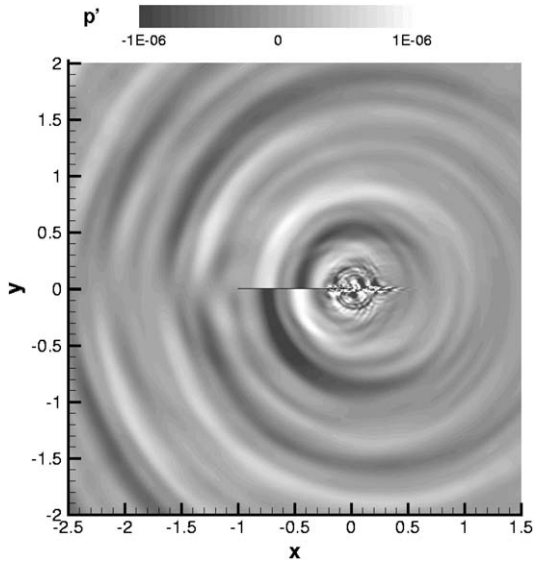

Fig. 7. Pressure contours of the trailing edge problem $M = 0.15$, $Re = 7 \times 10^5$ at time level $T = 3.0$, APE-4 solution on an acoustic grid with 2×10^5 points.

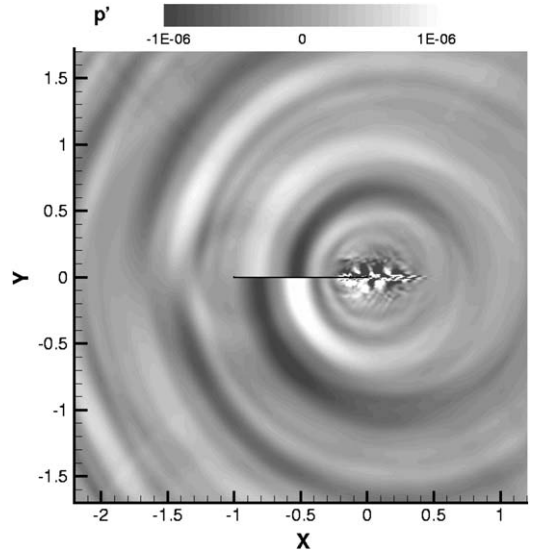

Fig. 8. Pressure contours of the trailing edge problem $M = 0.15$, $Re = 7 \times 10^5$ at time level $T = 3.0$, APE-4 solution on an acoustic grid with a 1.5^2 finer grid resolution compared to Fig. 7.

the PSD used here is based on the non-dimensionalized two-sided power spectral density per unit time [30]

$$\frac{\overline{p'^2}(\theta, r)}{c_\infty^2 \rho_\infty^4} = \int_{-\infty}^{\infty} \Phi(\theta, r, kl)\, \mathrm{d}kl. \tag{21}$$

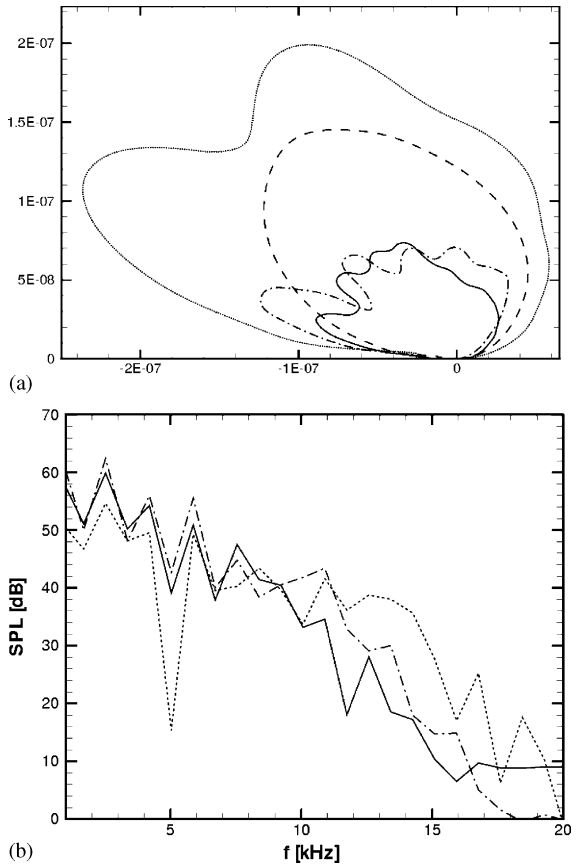

Fig. 9. Directivity $\Phi^{1/2}(\theta, r, kl)$ with $\Phi \triangleq$ non-dimensional power spectral density (PSD) of $\overline{p'^2}(\theta, r)/(\rho_\infty c_\infty^2)^2$, i.e., $\int_{-\infty}^{\infty} \Phi(\theta, r, kl)\,\mathrm{d}kl = \overline{p'^2}(\theta, r)/(\rho_\infty c_\infty^2)^2$; APE-4 simulation for $r = 1.5$, origin at the trailing edge, for various non-dimensional wave numbers $kl = 3.072$ (– – –), $kl = 9.215$ (···), $kl = 15.358$ (–·–), $kl = 21.502$ (——) (a); and sound pressure levels (SPL) for a receiving point in $r = 1.5$ above the trailing edge for directions $\theta = 90°$ (——), $\theta = 135°$ (–·–), and $\theta = 45°$ (···) (b).

The directivities agree qualitatively very well with the shapes of the approximate harmonic non-compact edge noise Green's function according to Howe [31,32]. In the compact limit the product of wave number and chord length tends to zero, i.e., $kl \to 0$. In this limit, the directivity recovers a dipole eight characteristic $\propto \sin(\theta)$. For the opposite case with $kl \to \infty$ the chord length to wavelength ratio tends to infinity, i.e., the cardioid directivity of the semi-infinite flat plate $\propto \sin(\theta/2)$ follows. With increasing wave numbers a multi-lobe pattern appears, whose envelopes converge against the cardioid shape.

In the acoustic analogy approach the acoustic far field follows from a convolution integral of the Green's function with the acoustic source, which is for the trailing edge problem compact and confined to the vicinity of the trailing edge. Hence, the convolution integral reduces in the frequency domain to the product of the harmonic non-compact edge noise Green's function times the frequency-dependent effective acoustic trailing edge source. In other words the Green's function yields the source directivity which is scaled by the spectral acoustic source strength. The

directivities of the acoustic simulation based on the hybrid approach that are depicted in Fig. 9 shows evidence of this dependence since the directivities agree qualitatively with the harmonic edge noise Green's functions of Howe but are scaled such that different magnitudes of the effective spectral pressure follow for the resolved frequencies. In particular for non-dimensional wave numbers larger than $kl = 9.215$ the magnitudes successively decay.

Fig. 9(b) depicts the PSD at three receiving points with a distance $r \approx 1.5$ to the trailing edge. The three receiving points are related to the polar angles $\theta = 45°$, $90°$, and $135°$, respectively, where all angles are defined similar to Fig. 1. The SPL and dimensional frequencies are computed based on the chord length and the ambient thermodynamic properties of the experimental setup. The dimensional pressure levels are related to a reference pressure of $p_{ref} = 2 \times 10^{-5}$ Pa, such that the SPL follows from

$$\mathrm{SPL}\ (dB) = 20 \log\left(\frac{p_{eff}}{p_{ref}}\right), \quad p_{ref} = 2 \times 10^{-5}\ \mathrm{Pa},$$

with $p_{eff} \coloneqq \rho_\infty c_\infty^2 \Phi^{1/2}$. The spectral distributions evidence the decline of the SPL over the frequency band.

6. Conclusion

A new hybrid prediction method based on an LES has been developed for the acoustic source region and acoustic perturbation equations for the time-dependent acoustic simulation. The results for the trailing edge problem are particularly encouraging. A vortex source based on Lamb's vector is proposed, which can be computed easily from a compressible LES.

Acknowledgements

This work was supported by the Deutsche Forschungsgemeinschaft (DFG) under Grant number SCHR 309/15.

References

[1] R. Ewert, M. Meinke, W. Schröder, Aeroacoustic source terms for the linearized Euler-equations, in: *Proceedings of the Sixth AIAA/CEAS Aeroacoustics Conference*, AIAA Paper 2000-2046, 2000.

[2] W.A. El-Askary, M. Meinke, W. Schröder, Towards the numerical analysis of trailing-edge noise, in: *DGLR German Aerospace Congress 2001*, DGLR Paper JT 2001-2176.

[3] R. Ewert, W. Schröder, Acoustic perturbation equations based on flow decomposition via source filtering, *Journal of Computational Physics* 188 (2) (2003) 365–398.

[4] R. Ewert, M. Meinke, W. Schröder, Comparison of source term formulations for a hybrid cfd/caa method, in: *Proceedings of the Seventh AIAA/CEAS Aeroacoustics Conference*, AIAA Paper 2001-2200, 2001.

[5] R. Ewert, M. Opiela, M. Meinke, W. Schröder, On the computation of the aeroacoustic sound generated by the turbulent flow behind a blunt trailing edge, *Computational Fluid Dynamics Journal* 9 (1) (2001) 306–316.

[6] A. Pierce, Wave equation for sound in fluids with unsteady inhomogeneous flow, *Journal of the Acoustical Society of America* 87 (6) (1990) 2292–2299.

[7] M. Goldstein, Unsteady vortical and entropic disturbances of potential flows round arbitrary obstacles, *Journal of Fluid Mechanics* 891 (1978) 433–468.
[8] V. Golubev, H. Atassi, Acoustic-vorticity waves in swirling flows, *Journal of Sound and Vibration* 209 (2) (1998) 203–222.
[9] A.J. Cooper, N. Peake, Propagation of unsteady disturbances in a slowly varying duct with mean swirling flow, *Journal of Fluid Mechanics* 445 (2001) 207–234.
[10] W. Möhring, A well posed acoustic analogy based on a moving acoustic medium, in: P. Költzsch, N. Kalitzin (Eds.), *Aeroacoustic Workshop*, 1999.
[11] W. Möhring, Modelling low Mach number noise, in: E.-A. Müller (Ed.), *Mechanics of Sound Generation in Flows*, Springer, Berlin, 1979.
[12] M. Howe, *Acoustics of Fluid–Structure Interactions*, Cambridge University Press, Cambridge, 1998.
[13] M.S. Howe, Contributions to the theory of aerodynamic sound, with application to excess jet noise and the theory of the flute, *Journal of Fluid Mechanics* 71 (4) (1975) 625–673.
[14] M.J. Lighthill, On sound generated aerodynamically: I. General theory, *Proceedings of the Royal Society of London Series A* 211 (1952) 564–587.
[15] S. Bergliaffa, K. Hibberd, M. Stone, M. Visser, Wave equation for sound in fluids with vorticity, LANL preprint cond-mat/0106255, 2001.
[16] A. Powell, Theory of vortex sound, *Journal of the Acoustical Society of America* 36 (1) (1964) 177–195.
[17] P. Morris, F. Farassat, Acoustic analogy and alternative theories for jet noise prediction, *American Institute of Aeronautics and Astronautics Journal* 40 (4) (2002) 671–680.
[18] E.-A. Müller, F. Obermeier, The spinning vortices as a source of sound, in: *AGARD CP-22*, 1967, pp. 177–195.
[19] C. Tam, J. Webb, Dispersion-relation-preserving finite difference schemes for computational acoustics, *Journal of Computational Physics* 107 (1993) 262–281.
[20] F.Q. Hu, M.Y. Hussaini, J.L. Manthey, Low-dissipation and low-dispersion Runge–Kutta schemes for computational acoustics, *Journal of Computational Physics* 124 (1996) 177–191.
[21] C. Tam, Z. Dong, A study of the short wave components in computational acoustics, *Journal of Computational Acoustics* 1 (1) (1993) 1–30.
[22] O. Vasilyev, A general class of commutative filters for LES in complex geometries, *Journal of Computational Physics* 146 (1998) 82–104.
[23] C. Tam, Z. Dong, Wall boundary condition for high-order finite-difference schemes in computational aeroacoustics, *Theoretical and Computational Fluid Dynamics* 6 (6) (1994) 303–322.
[24] M. Meinke, W. Schröder, E. Krause, T. Rister, A comparison of second- and sixth-order methods for large-eddy simulations, *Computers and Fluids* 31 (2002) 695–718.
[25] J. Ostertag, S. Guidati, S. Wagner, A. Wilde, N. Kalitzin, Prediction and measurement of airframe noise on a generic body, AIAA Paper 2000-2063, 2000.
[26] E. Manoha, C. Delahay, P. Sagaut, I. Mary, S. Khelil, P. Guillen, Numerical prediction of the unsteady flow and radiated noise from a 3D lifting airfoil, in: *Proceedings of the Seventh AIAA/CEAS Aeroacoustics Conference*, AIAA Paper 2001-2133, 2001.
[27] C. Kato, A. Iida, Y. Takano, H. Fujita, M. Ikegawa, Numerical prediction of aerodynamic noise radiated from low mach number turbulent wake, AIAA Paper 93-145, 1993.
[28] M. Wang, P. Moin, Computation of trailing-edge flow and noise using large-eddy simulation, *American Institute of Aeronautics and Astronautics Journal* 38 (12) (2000) 2201–2209.
[29] A.A. Oberai, F. Roknaldin, T.J.R. Hughes, Trailing-edge noise due to turbulent flows, Technical Report, Boston University, Report No. 02-002, 2002.
[30] W. Press, S. Teukolsky, W. Vetterling, B. Flannery, *Numerical Recipes in Fortran 77*, Cambridge University Press, Cambridge, 1996.
[31] M. Howe, Edge-source acoustic Green's function for an airfoil of arbitrary chord, with application to trailing edge noise, *Quarterly Journal of Mechanics and Applied Mathematics* 54 (1) (2001) 139–155.
[32] M. Howe, Flow–structure interaction noise at low Mach numbers, in: *Proceedings NATO RTO/AVT Symposium on Aging Mechanisms and Control, Part A—Development in Computational Aero- and Hydro-Acoustics*, Manchester, UK, 8–11 October 2001.